Available online at BCREC Website: https://bcrec.undip.ac.id

Bulletin of Chemical Reaction Engineering & Catalysis, 13 (2) 2018, 341-354

Research Article

Facile Synthesis and Characterization of Multi-Layer Graphene Growth on Co-Ni Oxide/Al_2O_3 Substrate Using Chemical Vapour Deposition

May Ali[a], Suraya Abdul Rashid[a,b,*], Mohd Nizar Hamidon[a,b], Faizah Md Yasin[a,b]

[a]*Chemical & Environmental Engineering Department, Faculty of Engineering, Universiti Putra Malaysia, 43400, Selangor, Malaysia*
[b]*Institute of Advanced Technology (ITMA), Universiti Putra Malaysia, 43400, Serdang, Selangor Darul Ehsan, Malaysia*

Received: 12nd August 2017; Revised: 15th February 2018; Accepted: 18th February 2018; Available online: 11st June 2018; Published regularly: 1st August 2018

Abstract

The synthesis and characterization of multilayer graphene (MLG) growth on bimetallic Co-Ni oxide/Al_2O_3 substrate using chemical vapour deposition (CVD) were investigated. The synthesis of MLG was performed at a temperature range of 700-900 °C. Characterization was carried out using TGA, XRD, FESEM, HRTEM, EDX, XPS, FTIR, and Raman spectroscopy. The MLG growth on the bimetallic substrate was confirmed by XRD, FESEM, and HRTEM analysis. TGA and Raman spectroscopy analyses indicate the formation of thermally stable and high-quality MLG. The kinetic growth of MLG was investigated by varying the reaction temperature and monitoring the partial pressure of the ethanol (C_2H_5OH) as well as that of hydrogen. The data obtained were fitted to the Langmuir-Hinshelwood kinetic model for the estimation of the reaction rate constants at different temperatures. The results showed that the reaction rate constant increased with temperature and the apparent activation energy of 13.72 kJ.mol^{-1} was obtained indicating a relatively fast rate of MLG growth. The parity plot obtained for the comparison of the predicted and observed rate of C_2H_5OH consumptions showed an excellent agreement. This study is important for understanding the growth kinetics of MLG in order to develop appropriate measures that can control the production of MLG thin films for use in the electronic industries.

Keywords: Alumina; Bimetallic Cobalt-Nickel Oxide; Chemical Vapour Deposition; Multi-Layer Graphene; Kinetics

How to Cite: Ali, M., Rashid, S.A., Hamidon, M.Z., Yasin, F.M. (2018). Facile Synthesis and Characterization of Multi-Layer Graphene Growth on Co-Ni Oxide/Al_2O_3 Substrate Using Chemical Vapour Deposition. *Bulletin of Chemical Reaction Engineering & Catalysis*, 13 (2): 341-354 (doi:10.9767/bcrec.13.2.1453.341-354)

Permalink/DOI: https://doi.org/10.9767/bcrec.13.2.1453.341-354

1. Introduction

There has been growing interest in the synthesis of graphene since the first published article in 2004 by Noselov *et al.* [1]. Graphene as a two-dimensional form of carbon with honeycomb-like lattice arrangement has been reported as the main building block for all categories of graphitic materials [2]. Graphene exhibit two-dimensional structure with distinct atomic and electronic properties which justify its appli-

* Corresponding Author.
E-mail: suraya@upm.edu.my (S.A. Rashid)

cation in electronics and photonics [3]. The growing interest in graphene applications as semiconductors in electronics can be attributed to its high carrier mobility (>100000 $cm^2.V^{-1}.s^{-1}$) as well as saturation velocities (the maximum attainable velocity a charge carrier in a semiconductor in the presence of very high electric field) (5×10^7 $cm.s^{-1}$) [4-6]. Furthermore, graphene has been reported to display excellent mechanical properties (stiffness and tensile strength), high thermal conductivity and high current carrying capacity [7,8]. Similarly, the application of graphene in photonics is primarily due to its excellent optical properties over a wide range of wavelengths without constraints such as local defects [9-11].

Graphene as a non-silicon based material has the potential of being a driving force in nanotechnology [12]. Its applications will help develop integrated circuits at a smaller scale comparable with that of silicon-based complementary metal-oxide-semiconductor (CMOS) technology [13,14]. Besides, graphene is characterized by excellent physicochemical properties such as a theoretically large surface area, high intrinsic mobility, high Young's modulus and thermal conductivity as well as high optical transmittance [15]. Its high specific surface area makes it appealing as a support for synthesis of metal based catalysts. Graphene-supported catalysts have been reported in reactions such as biomimetric oxidation, photocatalytic, decomposition of hydrous hydrazine, hydrogen production from silicon photocathode and enhanced electro-catalytic oxidation of methanol [16-18].

In most of the reported work on graphene synthesis, methods such as exfoliation and cleavage, chemical reduction of exfoliated graphite oxide and chemical vapour deposition (CVD) have been employed [19-21]. The exfoliation mechanism entails a process whereby graphene can be peeled from bulk graphite, layer by layer [22]. To achieve this, the resistance from Van der Wall's attraction between the adjacent sheets must be overcome. The application of mechanical exfoliation pioneers the discoveries of excellent electronic and mechanical properties of graphene [23]. However, one major challenge of the exfoliation technique is the low yields of graphene obtain from the process [24]. Graphitic materials can also be obtained by chemical reduction of graphene oxide [20, 25]. Reducing agents such as hydrazine hydrate is usually employed at a controlled temperature [26]. Often, the reducing agent is very toxic and hence poses health risks to the environment [27]. Besides, the use of extremely strong reducing agents (e.g. lithium aluminum hydride) has been problematic due to side reactions with dispersing solvents for graphene oxide [28]. Among the several methods reported in the literature, the synthesis of graphene from CVD is a more promising method for large scale production of graphitic materials [21]. Reports have shown that the diffusion of the carbon into the metal thin film is the main growth mechanism [29]. Although graphene (also known as single layer graphene) has excellent properties for several applications, there is growing interest in the application of multilayer graphene (MLG) in the field of material science and engineering. MLG can best be defined based on its applications and physical properties. According to its electrical properties, a material is considered to be MLG if it is thin enough to have its carrier density tuned via the electrostatic gating. Also, based on its thermal properties, if the material has a unique Raman spectrum from that of the bulk graphite, such material is considered to be MLG [30]. Also, MLG is a graphene thin films of weak Van der Waals interaction between its layers that show excellent electronic properties with high potential for sensing application.

The growth of MLG on metals, such as: Ir, Ni, Rh, Cu, Pt, Pd, and Co by CVD, has been extensively studied with their corresponding growth mechanisms [31]. In all of these studies, the formation of MLG was reported to be by the nucleation of the active carbon species which resulted from the decomposition of the precursors on the surface of the metal catalysts. Also, MLG growth has been investigated on substrates, such as: Si, W, Mo, SiO_2, Al_2O_3, using CVD [32]. Ogawa *et al.* [33] investigated growth on Cu/Al_2O_3 substrate using CVD method. The authors' findings show that the amount of diffused carbon into the Cu on Al_2O_3 substrate using the CVD was small. This is attributed to the low solubility of the carbon by the Cu catalyst. However, the growth of MLG using bimetallic Co-Ni oxide catalyst via CVD method has not been reported to the best of the author's knowledge.

In the present study, the Al_2O_3 serves as a support to the Co-Ni oxide bimetallic catalyst. The combination of the bimetallic Co-Ni oxide with the Al_2O_3 will be referred to as Co-Ni oxide/Al_2O_3 substrate henceforth. One important feature of the Co-Ni oxide as a catalyst for MLG synthesis is its tendency to facilitate high carbon solubility (approximately 0.052 wt%) [32]. Moreover, the kinetics of the MLG growth on Co-Ni oxide/Al_2O_3 substrate using CVD has also not been investigated. This study, there-

fore, focuses on the synthesis, characterization and the kinetics of MLG growth on Co-Ni oxide/Al_2O_3 substrate using CVD. It is of great importance to investigate the kinetics of the MLG growth because the quantity of carbon dissolution during CVD is a function of the precursor's partial pressure and the deposition time.

2. Materials and Methods

2.1 Functionalization of substrate

MLG film was formed by epitaxial growth on Co-Ni oxide/Al_2O_3 substrate. Prior to Co-Ni oxide deposition, the alumina substrate was acid treated first to etch the inherently smooth surface. The solution for the substrate functionalization was prepared by mixing 50 mL HNO_3, 5 mL H_2SO_4, and 500 mL H_2O in an Erlenmeyer flask and placed in a mechanical shaker for 30 min. Subsequently, about 0.65 g of the Al_2O_3 (1.5×1.5 cm^2) substrate was functionalized by immersing in the as-prepared solution for 7 days in order to allow surface etching for the deposition of the Co-Ni oxide/Al_2O_3 substrate. Thereafter, the functionalized Al_2O_3 substrate was washed with de-ionized water to remove any residual acids or traces of impurities. This was followed by drying the Al_2O_3 substrate in an oven at 110 ^oC for 1 h.

2.2 Catalyst preparation

Nickel(II) nitrate hexahydrate (99.99 % trace metal basis, Sigma-Aldrich) and cobalt(II) nitrate hexahydrate (99.99 % trace metal basis, Sigma-Aldrich) in different proportions were utilized as the catalysts precursors. The nickel(II) nitrate hexahydrate and cobalt(II) nitrate hexahydrate were mixed with 50 mL of ethanol and sonicated for 24 h. The obtained catalyst suspension was then drop-casted onto the alumina substrate and dried on a hot plate at 110 ^oC for 4 h, and thereafter oven dried for 24 h at 110 ^oC.

2.3 Catalyst and MLG characterization

Several characterization techniques were employed to determine the properties of the Co-Ni oxide/Al_2O_3 substrate. Thermogravimetric Analysis (TGA) was performed using thermogravimetric analyzer (TA instrument, Q50) under a high purity N_2 (($99.5\ \%\ N_2$, $0.5\ \%\ O_2$) atmosphere with the temperature being controlled from 50 to 1000 ^oC at a heating rate of 10 ^oC/min. The phase identification and crystallinity of the as-prepared catalyst and MLG were characterized by X-ray powder Diffraction (XRD) analysis (RIGAKU mini flex II X-ray diffractometer) from 3 to 145^o 2θ scanning range. The X-ray source was Cu Kα with wavelength (λ) of 0.154 nm radiation. The surface morphology of the MLG film was characterized by Field Emission Scanning Electron Microscopy (FESEM) (JSM 7800F). The crystallographic structure of the graphene formed was measured using High-Resolution Transmission Electron Microscope (HRTEM) (JEOL Pte Ltd Japan). The Selected-Area Electron Diffraction (SAED) pattern was obtained for the MLG growth from a bundle of the MLG randomly deposited on the TEM grid. The chemical groups of the MLG was determined using Fourier Transform Infra Red (FTIR) spectroscopy. The spectra were collected at wave number ranging from 4000-400 cm^{-1} using a resolution of 8 cm^{-1}. X-ray Photoelectron Spectroscopy (XPS) of the MLG was performed using an Omicron ESCA Probe (Omicron Nanotech, Germany). The XPS which has monochromatic Al-Kα radiation source (hv =1486.6 eV) employs Kratos Vision 2.2 software for curve fittings and the calculation of the atomic concentrations.

2.4 MLG synthesis by Chemical Vapor Deposition (CVD)

The Co-Ni oxide/Al_2O_3 substrate was weighed (15 g) then loaded into a quartz tube placed horizontally in a furnace. The quartz tube was initially purged with argon at a temperature of 700 ^oC. The MLG growth was initiated by measuring a known amount of ethanol in a conical flask which was heated to allow the formation of ethanol vapour. The ethanol vapour was carried into the CVD reactor using Argon gas. The final weight of the catalyst together with the MLG formed was measured in order to estimate the yield of MLG formed. Furthermore, the kinetics measurement was performed by varying the partial pressure of the ethanol and that of the hydrogen at a temperature range of 700-900 ^oC under atmospheric condition for 2 h. The outlet gasses from the CVD were detected using online gas chromatography coupled with thermal conductivity detector and flame ionization detector (GC-TCD-FID-7820 A, Agilent Technologies.

3. Results and Discussions

3.1 Characterization of the MLG

Thermogravimetric analysis (TGA) analysis was carried out to investigate the thermal stability of the MLG and the decomposition pattern of residues. The TGA and Differential

Thermo Gravimetric (DTG) profiles of the sample at 700 and 800 °C are depicted in Figure 1. Based on the TGA profile of the samples at 700 °C (Figure 1a), it was observed that there were weight losses between 100-400 °C which could be due to evaporation of physical and crystallized water from the catalyst's precursor [34]. The sharp weight loss at 540 °C represented by the sharp DTG curve depicts a rapid weight loss that can be attributed to the oxidation of carbon into gaseous carbon dioxide. This is consistent with the report of Liu *et al.* [35] and Zhao *et al.* [36] who reported that weight loss due to carbon oxidation occurs at a temperature range of 400-680 °C. Conversely, the TGA analysis of the sample at 800 °C (Figure 1b) shows a stable trend until 500 °C. However, there was a sharp weight loss at 580 °C which a can also be attributed to the carbon oxidation by the traces of O_2 in the N_2 [35-36]. The weight gained at 650 °C could be as a result of the oxidation of the Co and Ni metals into solid oxides as reported by Liu *et al.* [35]. At a temperature greater than 650 °C, there were no other species traces present in both samples as observed from the DTG curve. The carbon yields were estimated from the TGA profile at 700 and 800 °C as 60 and 70 %, respectively. The shift in the carbon oxidation temperature from 540 (for MLG growth at 700 °C) to 580 °C (for MLG growth at 800 °C) implies that a better sp^2 network structure which cannot be easily degraded is obtained in MLG growth at 800 °C compared to that obtained at 700 °C. Also, a higher purity of MLG formed at 800 °C is expected compared to that formed at 700 °C. This result can be corroborated with the XPS spectra of the MLG depicted in Figure 5 Which show a high intensity of the C-C bond for the MLG growth at 800 °C compared to that of 700 °C [37].

The XRD pattern of the synthesized MLG at 700 and 800 °C are shown in Figure 2. The XRD pattern displayed different diffraction

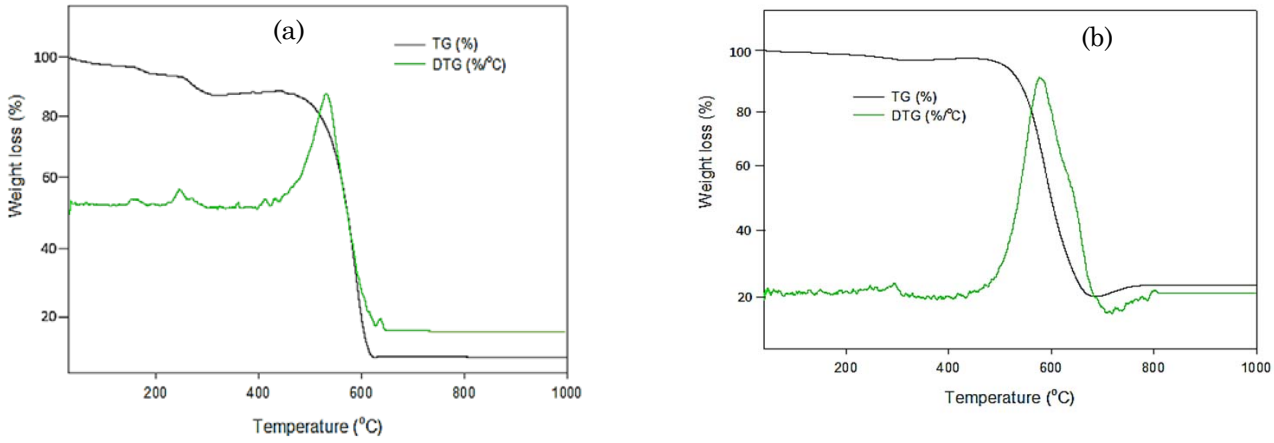

Figure 1. TGA profile for the as-synthesized MLG at (a) reaction temperature of 700 °C (b) reaction temperature of 800 °C

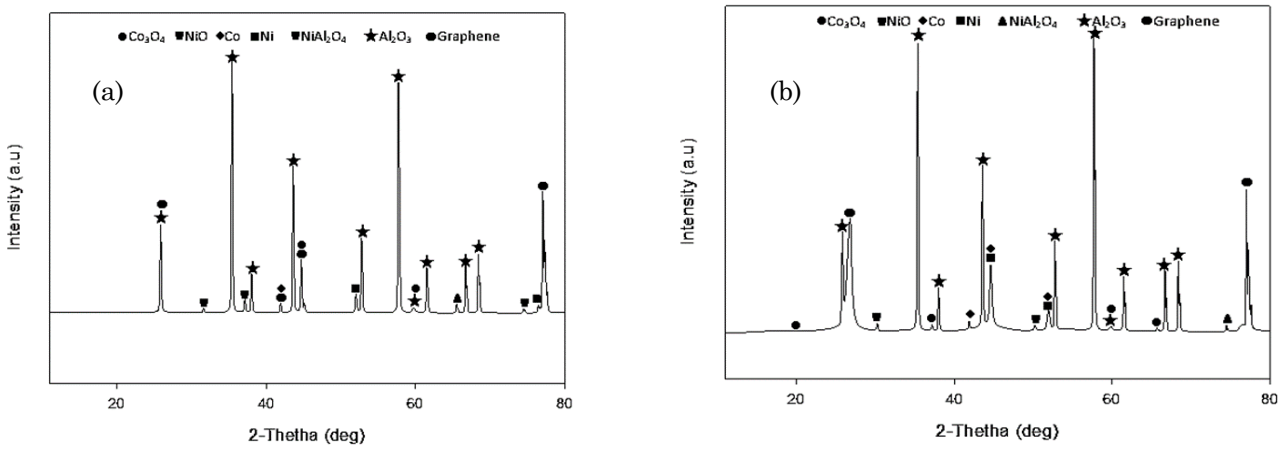

Figure 2. XRD pattern of the as-synthesized MLG on Co-Ni oxide/Al_2O_3 substrate (a) 700 °C (b) 800 °C

peaks, clearly distinguishing the different components in the analysed sample. For the MLG synthesized at 700 °C, the peaks at 2θ = 25.44, 41.89 and 77.54° can be attributed to the growth of MLG (indicated as graphene in Figure 2a) (ICDD No: 000010640). While the peaks at 2θ = 38.50, 44.157, 53.32, 58.20, 62.06, 68° corresponds to Al_2O_3 (ICDD No: 00001124340). For the MLG synthesized at 800 °C, the peaks at 2θ = 26.44° and 77.028° can be attributed to the growth of MLG (ICDD No: 000010640) (indicated as graphene in Figure 2b). While the peaks at 2θ = 25.82, 35.35, 37.99, 43.54, 52.70, 57.68, 58.82, 61.46, and 76.26°, corresponds to Al_2O_3 (ICDD No: 00001124340). The deposited Ni catalyst on the Al_2O_3 substrate leads to the formation of $NiAl_2O_4$ compound at 2θ = 44.15° and 2θ = 76.25° for 700 and 800 °C, respectively, as indicated by the XRD pattern in Figures 2a and b.

The catalyst active phases represented by the Co and Ni crystallites are observed at 2θ = 41.87, 51.90, 76.25°, and 2θ = 44.58, 51.90, 76.25°, respectively (Figure 2). The occurrence of the Co and Ni crystallite in the XRD pattern could be as a result of the partial reduction of Co_3O_4 and NiO by the H_2 gas evolved during the dehydrogenation of the ethanol in the CVD as shown in the Equations (1) and (2).

$$Co_3O_4 + H_2 \rightarrow 3CoO + H_2O \quad (1)$$

$$CoO + H_2 \rightarrow Co + H_2O \quad (2)$$

$$NiO + H_2 \rightarrow Ni + H_2O \quad (3)$$

The Co_3O_4 (ICDD No: 000090418) and NiO crystal phases can be identified at 2θ = 20.00, 37.21, 65.69°, and 2θ = 29.74 and 42.45°, respectively. It can be seen that a higher intensity of the MLG is observed at 2θ = 77.028° for 800 °C compared to the intensity of the MLG observed at 2θ = 77.54° for 700°C. The higher intensity at 800 °C implies that the increase in temperature stimulate more growth of the MLG. The average crystallite size of the MLG at 700 and 800 °C were obtained as 66.86 nm and 12.73 nm, respectively, using Scherrer equation (4) [38].

$$D = \frac{K\lambda}{B\cos\theta} \quad (4)$$

where D is the average crystallite size, K is the shape factor = 0.9, λ is 0.15406 nm, θ is the Bragg angle, and B is the full width at half maximum.

The differences in the crystallite size obtained at 700 and 800 °C could be attributed to the increase in the sp^2 domain size from 0.788 nm (obtained at θ = 77.54°) to 0.791 nm (obtained at θ = 77.03°) with compacted interlayer spacing which is consistent with the FE-SEM images shown in Figures 4 (a) and (b) [39]. As the temperature increases more defects is being removed thereby enhancing the sp^2 domain of the MLG. The presence of the sp^2 domain in the MLG could be very useful for graphene-based electronic devices and other applications. Besides, the smaller crystallite size of the MLG obtained at 800 °C is also essential for gas sensor application in that the adsorption potential of the MLG is enhanced [40].

The smaller crystallite size of the MLG obtained at 800 °C is essential for gas sensor application in that the adsorption potential of the MLG is enhanced [40]. The MLG with small crystallite size will facilitate the adsorption of gasses on the MLG and result in charge transfer between adsorbed molecules and the MLG [41]

The interlayer spacing for the MLG growth at 700 and 800 °C were estimated from Bragg's equation (5) as 0.788 and 0.791 nm respectively. A lower *d*-spacing value of 0.36 nm has been reported for MLG by [42]. The higher d-spacing value obtained for the MLG synthesized in this study could be as result of the compactness of the graphene layer. It can be seen that the *d*-spacing value of the MLG synthesized at 800 °C is higher compared that of 700 °C, which implies that the graphene layer at 800 °C is more compacted than that of 700 °C which is more for the MLG synthesized at 800 °C compared to that of 700 °C.

$$d = \frac{\lambda}{2\sin\theta} \quad (5)$$

where d is the interlayer spacing in nm.

HRTEM was used to investigate the morphology of the Co-Ni oxide catalyst. It can be seen from the HRTEM images (Figure 3a) the presence of the Co and Ni crystals. The formation of truncated polyhedron shaped Co and Ni nanoparticles with high-index facets is visible from the HRTEM image. The elemental composition of the Co-Ni oxide catalyst obtained from the EDX analyses is depicted in Figure 3. The EDX micrograph shows the peaks corresponding Ni, Co, and O elements which are a confirmation of the presence of the drop-casted bimetallic Co-Ni and their oxides.

The elemental composition and morphology of the as-synthesized MLG at 700 and 800 °C was investigated using, FESEM, HRTEM, and EDX as shown in Figure 4. The EDX micrograph (Figure 4 (g)) confirmed the deposition of

the MLG on the Co-Ni oxide/Al_2O_3 substrate as a representation by different percentage weight composition of C (85.98 %), O (4.65 %), Al (4.08 %), Co (0.15 %) and Ni (5.06 %). Also, a close observation of the FESEM image (Figures 4 (a) and (b)) show that the MLG formed are uniformly grown with hundredth of nanometres in thickness. Moreover, the images showed large MLG sheets were grown on the Co-Ni oxide/Al_2O_3 substrate, which is transparent and having a stable feature under the electron beam. The lesser MLG film observed at 700 °C compared to the MLG film at 800 °C could be attributed to fewer graphene layers formed which are consistent with the values of I_{2D}/I_G (0.84 for MLG gown at 700 °C and 0.80 for MLG grown at 800 °C). Moreover, this also confirms the smaller crystallite size from the XRD analysis obtained for the MLG at 800 °C compared to that of 700 °C. The SAED images of the MLG shown inset in Figures 4 (c and d) confirms a faced-cubic-centre structure. The elemental composition of the MLG (indicated as C) and the Co-Ni oxide/Al_2O_3 substrate (indicated as Co, Ni, Al, and O) is depicted in Figure 4 (g).

The C1s XPS spectra and the full scan of the as-synthesized MLG are depicted in Figure 5. Gaussian-Lorentzian model was employed to perform the curve fittings of the C1s spectra after an initial Shirley background correction. Five types of bonding namely C=C, C–O, C=O, C–C and COOH can be identified from the XPS spectra at 700 and 800 °C (Figure 5 (b) and (d)). For MLG synthesized at 700 °C, the binding energy of the C=C, C–O, C=O, C–C, and COOH are assigned at 284.62, 285.30, 286.72, 288.52, and 290.90 eV, respectively, (Figure 5a). These bonds indicate the different atomic concentrations of the MLG and the catalyst components. The C1s peak (Figure 5d) of the MLG corresponds with that reported by Choudhury et al. [43]. Also, the C1s XPS spectra and the full scan of the MLG formed at 800 °C is depicted in Figures 5 (a) and (c). The binding energy of the C=C, C–O, C=O, C–C, and COOH are assigned at 284.92, 285.80, 286.96, 288.72, and 291.10 eV, respectively, which are in close range with that obtained at 700 °C. The appearance of the C–C bond at 284 eV is an indication that the MLG contains sp^2 hybridized carbon atoms which are an advantage for gas sensing application [44]. While the –C–O represent the sp^3 hybridized carbon. The atomic concentrations obtained at 700 and 800 °C (embedded Tables in Figures 5 (a) and (c) shows that a higher C1s was obtained at 800 °C compared to that of 700 °C which is an indication of temperature effect of the formation of MLG. It can be seen that the atomic concentration of Ni drastically decreased from 0.45 to 0.08 while there is just slight variance between the atomic concentration of Co at 700 °C and 800 °C. The difference in the atomic concentration of the Ni at 700 °C and 800 °C could be attributed continuous deactivation of the Ni active site by the growth of the carbon.

Previous work has reported that the Ni active site is susceptible to deactivation by carbon deposition which justifies the use of the bimetallic Co-Ni oxide in this study. The sp^2 domain size in the MLG growth at 700 °C and 800 °C was measured using the Tuinstra-Koenig relation $I_D/I_G = C(\lambda)/L_a$, where $C(\lambda) = 38.0$ (for peak-to-peak intensities, $\lambda = 632.7$ nm) [45]. The sp^2 domain size (L_a) for the MLG growth at 700 °C and 800 °C were estimated as 4.04 nm and 4.22 nm, respectively from the Raman spectroscopic analysis. Moreover, the O1s atomic concentration was also ob-

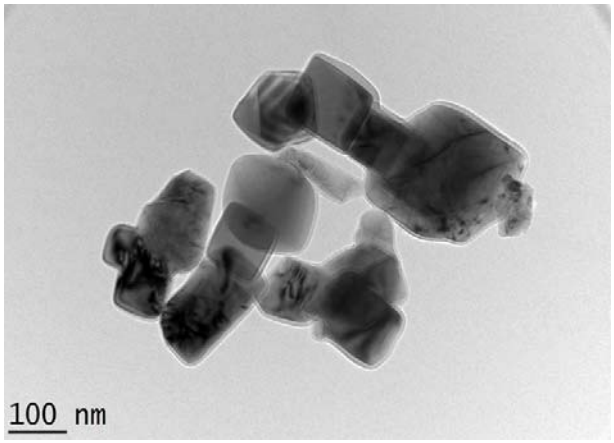

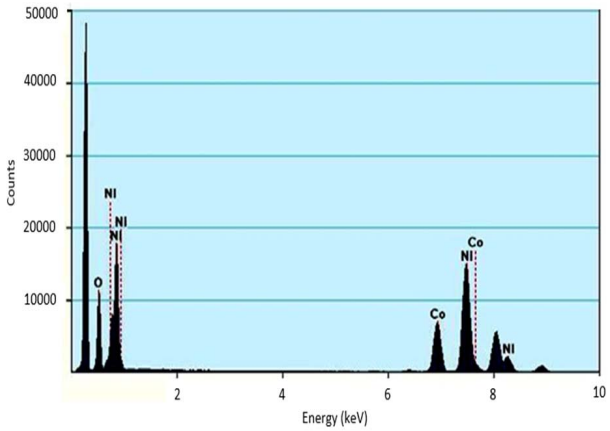

Figure 3. (a) The HRTEM image of the Co-Ni oxide catalyst, (b) EDX micrograph (insert is the dot mapping of the Ni, Co, and O)

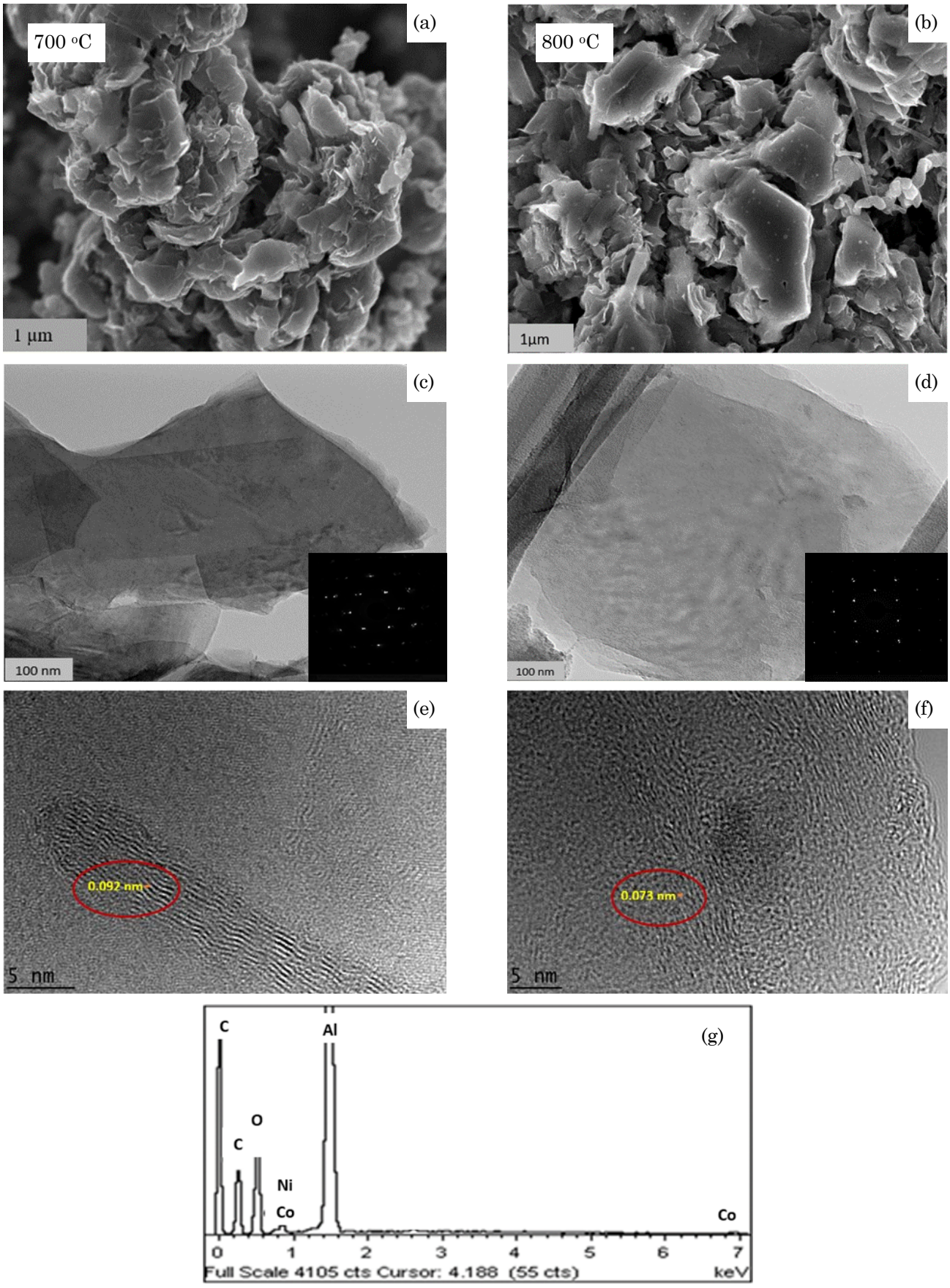

Figure 4. (a) FESEM image of the MLG at 700 °C and (b) FESEM image of the MLG at 800 °C (c)HRTEM image of the MLG at 700 °C (d) HRTEM image of the MLG at 800 °C (e) HRTEM image with d-spacing at 700 °C (f) HRTEM image with d-spacing at 800 °C (g) EDX micrograph

served to decrease from 8.86 to 4.53 % possible due to the loss of O_2 from the Co_3O_4 and NiO as the temperature increases.

Figure 6 shows the FTIR spectra of the MLG at 700 and 800 °C. Interestingly, the two IR spectra are identical which implies that the chemical bonds of the MLG were not affected by the changes in temperature. From the spectra, peaks at 540, 1450-1560, 2000-2350, and 3400-3550 cm^{-1} can be observed. The peak at 540 cm^{-1} can be attributed to inter-atomic vibration metal oxide (M–O) bond which signifies the presence of Ni–O and Co–O in the catalyst. The peaks at wave number 1450-1560 cm^{-1} can be assigned to stretching vibrational C=O bond which signifies the presence of oxygenated functional group as confirmed by the XPS analysis in Figure 5 [46]. The peaks at wave number 2000-2350 cm^{-1} can be assigned to stretching vibration C=C bond which signifies the formation of the MLG on the bimetallic Co-Ni oxide/Al_2O_3 substrate. The peaks at 3400-3550 cm^{-1} can be attributed to the stretching vibration O–H bond which implies the presence of adsorbed moisture. The high intensity of the C=C bond at 800 °C implies that

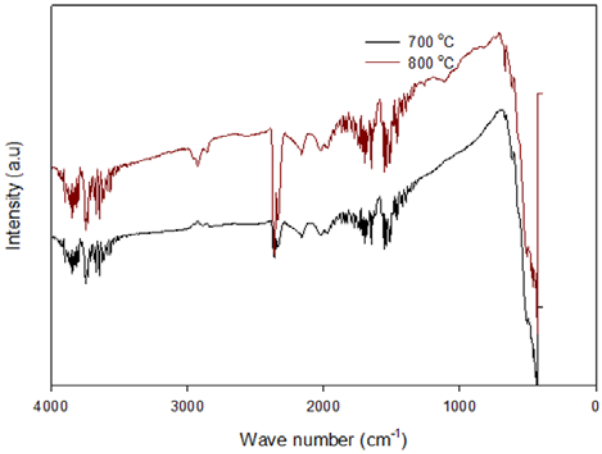

Figure 6. FTIR spectra of the MLG growth on Co-Ni oxide/Al_2O_3 substrate

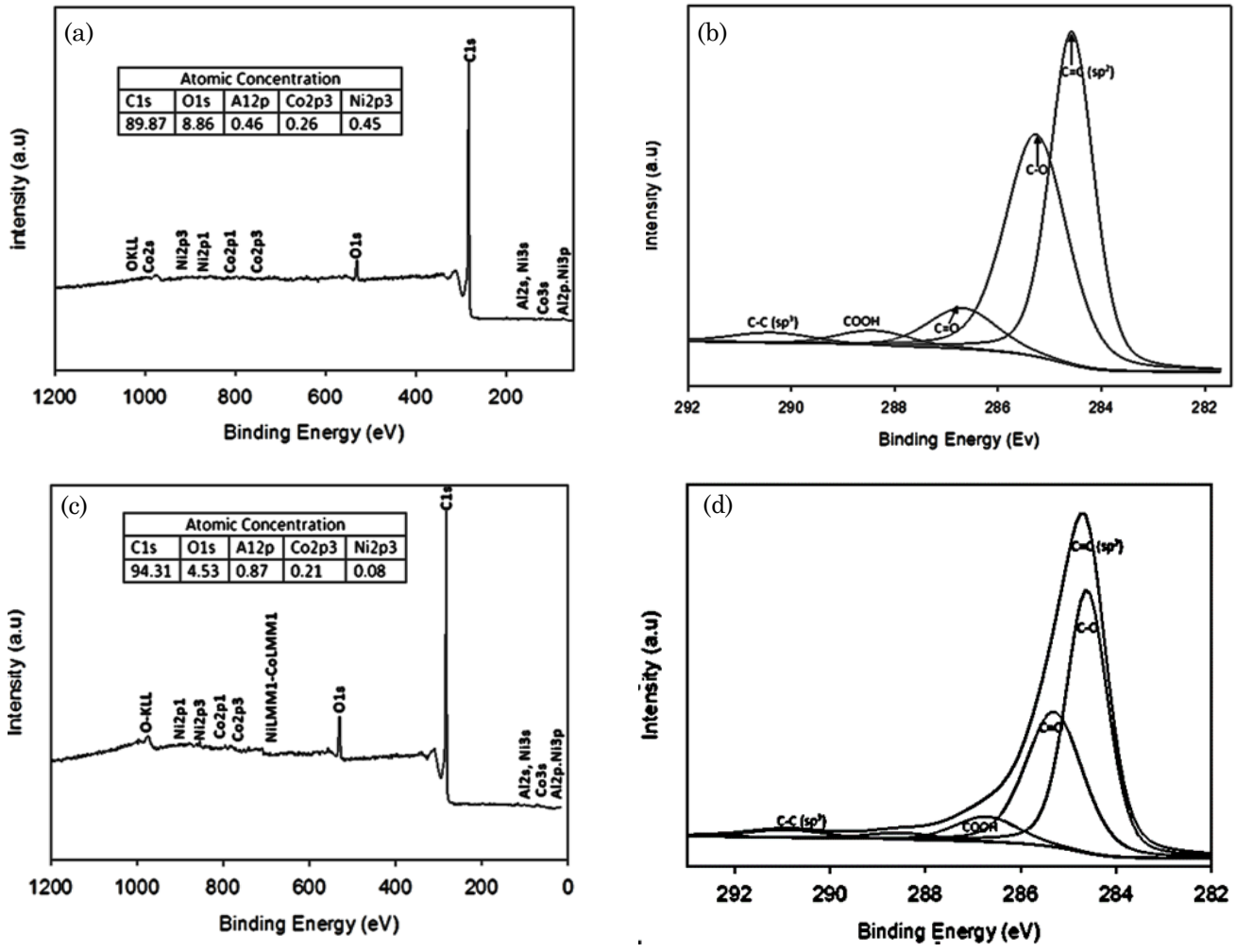

Figure 5. XPS spectra of the MLG growth at 700 °C (a) full (b) narrow scan 800 °C (c) full (d) narrow scan

increase in temperature stimulates the growth of the MLG on the bimetallic catalysts.

The Raman spectra showing the characteristic D, G and 2D peaks associated with MLG nanostructures are depicted in Figure 7. The D peaks can be identified at 1352 and 1341 cm^{-1} for the MLG growth at 700 and 800 °C respectively. The G peaks occur at 1586 and 1568 cm^{-1} for the MLG growth at 700 and 800 °C respectively. The 2D peaks which appear at 2701 and 2674 cm^{-1} for the MLG growth at 700 and 800 °C respectively depicts the multilayer nature of the graphene.

It is well known that the Raman spectra of pristine graphene contain only G and 2D [47]. The occurrence of D peaks in the Raman spectra of the MLG synthesized in this study shows the presence of edges [48, 49]. However, the intensity of the G peaks is higher compared to that of the D peaks as shown in Table 1, an indication of a good quality MLG as reported by Niilisk *et al.* [50]. Interestingly, the I_D/I_G values of 0.94 obtained at 700 °C is higher than 0.90 for the MLG at 800 °C. This implies that the MLG at 800 °C contained more sp^2 fragments compared to that of 700 °C [34]. The changes in the CVD temperature from 700 to 800 °C cause a slight shift in the G and 2D peaks positions of the Raman spectra of the MLG. This shift can be explained regarding increased inharmonic coupling of phonons (collective excitations in the arrangement of the C–C bond of the MLG) and increased thermal expansion (expansion resulting from changes in temperature) in the lattice of the MLG as reported by Calizo *et al.* [39]. A typical graphene has one free lattice parameter whose temperature dependence is characterized by linear thermal expansion. The I_{2D}/I_G values of 0.84 and 0.80 obtained at 700 and 800 °C, respectively, confirmed the multilayer nature of the graphene according to the report of Nguyen *et al.* [51] who stated that, $I_{2D}/I_G < 1$ is typical of a multilayer graphene. The lower I_{2D}/I_G value of 0.80 implies that the MLG obtained at 800 °C is thicker compared to that at 700 °C [48].

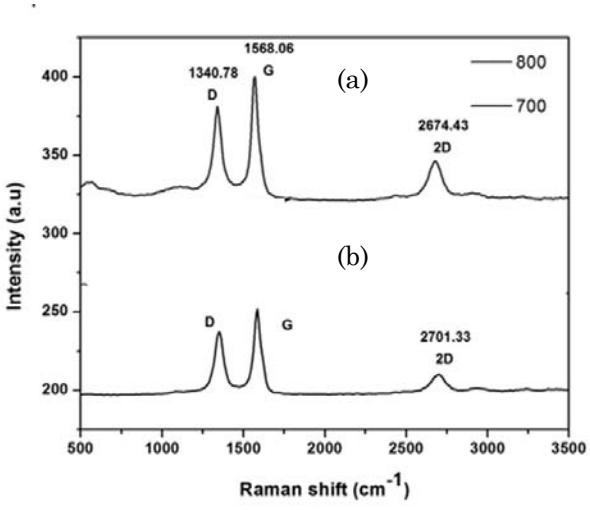

Figure 7. Raman Spectra of the MLG at (a) 800 °C and (b) 700 °C

3.2 Kinetic study

The kinetics of MLG growth on bimetallic Co-Ni oxide/Al_2O_3 substrate was investigated as a function of temperature and partial pressure of C_2H_5OH and H_2 as shown in Table 2. The kinetic study is aimed to investigate the influence of the partial pressures of the C_2H_5OH and H_2 on the MLG growth. In other words, the energy barrier to the growth of the MLG using CVD can be deduced from the kinetic studies. The rate of consumption of the C_2H_5OH ($-rC_2H_5OH$) is estimated from Equation (5):

$$-rC_2H_5OH = \frac{X_{C_2H_5OH} \cdot F_{C_2H_5OH}}{W} \quad (5)$$

where X_{C2H5OH} is the conversion C_2H_5OH, F_{C2H5OH} is the molar flow rate of the C_2H_5OH, and W is the weight of the catalyst which equal to 15 g.

The experimental data in Table 2 were fitted into Langmuir-Hinshelwood (L-H) kinetic model (Equation 6) based on the assumption that surface reaction is the rate determining step. A non-linear Levenberg-Marquardt algorithm in POLYMATH software was employed to calculate the k_{rxn} at different reaction temperatures [52] which are shown in Table 3. Careful observation of the results show that the reaction rate constant (K_{rxn}) increases with increase in temperature which is a typical characteristic of a temperature dependent re-

Table 1. Raman spectra analysis of the MLG formed at 700 and 800 °C

T (°C)	D band	G band	2D band	I_D/I_G	I_{2D}/I_G
700	1352	1586	2701	0.94	0.84
800	1341	1568	2674	0.90	0.80

action [53]. The values of the k_{rx}n were estimated from the L-H model as 0.0028, 0.0050, 0.0091, and 0.0500 for 700, 750, 800, and 900 °C, respectively.

$$r_{C_2H_5OH} = \frac{k_{rxn}.P_{C_2H_5OH}.P_{H_2}}{\left(1+K_{C_2H_5OH}P_{C_2H_5OH}+\sqrt{K_{H_2}P_{H_2}}\right)^3} \quad (6)$$

The kinetic parameters obtained from the L-H model were employed to obtain predicted the rate of consumption of C_2H_5OH to determine to what extent is the energy barrier in the formation of MLG by CVD overcome. The observed values of consumption rate of C_2H_5OH as well as the predicted rate from the Langmuir-Hinshelwood model were compared as shown in the parity plot depicted in Figure 8. The results show that the predicted C_2H_5OH consumption rate closely matches with the observed values except for few points. This implies that the experimental data can be fitted by Langmuir-Hinshelwood kinetic model. It can be inferred from the LH model that the rate of ethanol consumption for the CVD strongly influences the rate of MLG growth. As the partial pressure of the ethanol increases, the rate of MLG growth on the bimetallic also increases, an indication that there were minimal energy barriers that influence the MLG growth on the catalyst.

The rate data obtained from the kinetic studies at a temperature range of 700-900 °C was used to calculate the apparent activation energy required for the formation of the MLG

Table 2. The experimental data employed for kinetics modelling using Langmuir-Hinshelwood (L-H) expression

Temperature (°C)	r_{C2H5OH} (mmol/gcat/min)	P_{C2H5OH} (kPa)	P_{H2} (kPa)
700	4.11×10^{-5}	0.0370	0.8838
700	2.95×10^{-5}	0.0265	0.8523
700	10.7×10^{-5}	0.0963	0.8766
700	4.32×10^{-5}	0.0389	0.8963
700	2.17×10^{-5}	0.0196	0.883
750	3.31×10^{-5}	0.0298	0.8715
750	6.5×10^{-5}	0.0587	0.8994
750	8.07×10^{-5}	0.0726	0.8517
800	2.44×10^{-5}	0.0220	0.9069
800	3.29×10^{-5}	0.0296	0.8774
800	2.54×10^{-5}	0.0228	0.8967
800	5.80×10^{-5}	0.0052	0.2235
800	2.75×10^{-5}	0.0248	0.2889
900	3.02×10^{-5}	0.0272	0.3792
900	3.02×10^{-5}	0.0272	0.4637
900	3.02×10^{-5}	0.0272	0.5100
900	3.02×10^{-5}	0.0272	0.5030

Table 3. Kinetic parameters obtained from Langmuir-Hinshelwood model

Temperature (°C)	K_{rxn}	$K_{C_2H_5OH}$	K_{H_2}
700	0.0028	9.3164	0.0299
750	0.0050	0.0587	1.3240
800	0.0091	1.5750	2.0110
900	0.0500	31.2900	3.9040

on the Co-Ni oxide/Al_2O_3 substrate. The rate data (Table 2) were recorded after 2 h of reaction to ensure steady state performance of the catalyst. The data in Table 2 were fitted into Arrhenius expression (Equation 7).

$$\ln k = \ln A - \frac{E_a}{RT} \quad (7)$$

This is to enable the calculation of the apparent activation energy, E_a required to overcome the energy barrier during the MLG synthesis. Figure 9 shows the Arrhenius plots for the estimation of the apparent activation energy. The apparent activation energy of 13.73 kJ.mol^{-1} was obtained for the rate of consumption of C_2H_5OH which signifies a very fast rate of MLG growth on the catalyst. Moreover, since the E_a is > 10 kJ.mol^{-1}, it implies that the energy barrier to the growth of the MLG was strongly reduced by the presence of the bimetallic Co-Ni oxide/Al_2O_3 substrate [54]. The value of the E_a obtained in this study is lower compared to 201 and 164 kJ/mol reported by Losurdo *et al.* and Kim *et al.* [55,56], respectively for the synthesis of graphene using Cu and Ni catalysts by CVD. The variation in the E_a values could be as result of the different carbon sources employed for the studies as well as the catalytic system. In the Kim *et al.* and Losurdo *et al.* reports, CH_4 was used as the carbon source while C_2H_5OH is use in the present study. The high coefficient of (R^2) value of 0.976 obtained from the Arrhenius plot is an indication of the excellent fit of the experimental data to the Arrhenius equation.

4. Conclusion

The synthesis and characterization of MLG growth on bimetallic Co-Ni oxide/Al_2O_3 substrate by CVD have been investigated. The characterization results by Raman spectroscopy and other instrumental techniques showed evidence of the formation of MLG on the surface of the Co-Ni oxide/Al_2O_3 substrate by CVD. The I_{2D}/I_G values of 0.84 and 0.80 obtained for the MLG grown at 700 and 800 °C were < 1 as an indication that multilayer graphene was synthesized on the Co-Ni oxide/Al_2O_3 substrate. Also, the decrease in the I_D/I_G ratio from 0.94 to 0.90 implies an increase in the size of the sp^2 cluster of the MLG. In order to obtain the kinetic parameters, rate data were measured by varying the partial pressure of the C_2H_5OH vapour that flows into the CVD reactor and the CVD temperature from 700-900 °C. The rate data obtained were fitted into Langmuir-Hinshelwood model to estimate the kinetic parameters. The rate constants of 0.0028, 0.00504, 0.0091, and 0.0500 were obtained at 700, 750, 800, and 900 °C, respectively. The fitting of the kinetic data into Arrhenius plot resulted in an activation energy of 13.72 kJ.mol^{-1}, an indication of the fast rate of MLG growth on the Co-Ni oxide/Al_2O_3 substrate with a little energy barrier. This further affirms a rate controlled reaction process for the MLG growth via CVD. In the eventuality of scale-up process, the kinetic parameters (reaction rate constants and the activation energy) obtained in this study will help to provide measures in controlling the process conditions, such as: reaction temperature and the flow rate

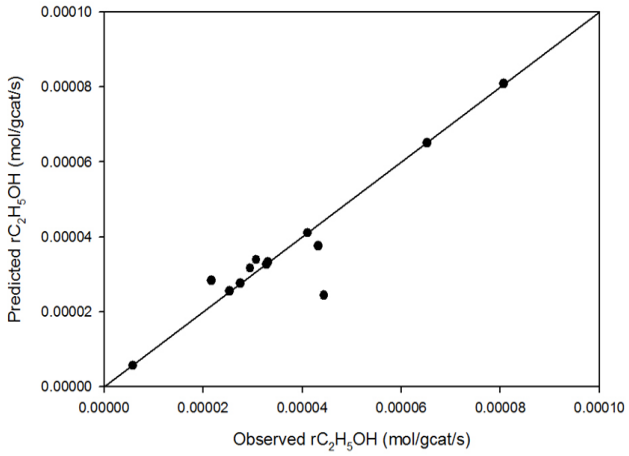

Figure 8. Parity plot showing the comparison between the observed and the predicted rate of consumption of C_2H_5OH

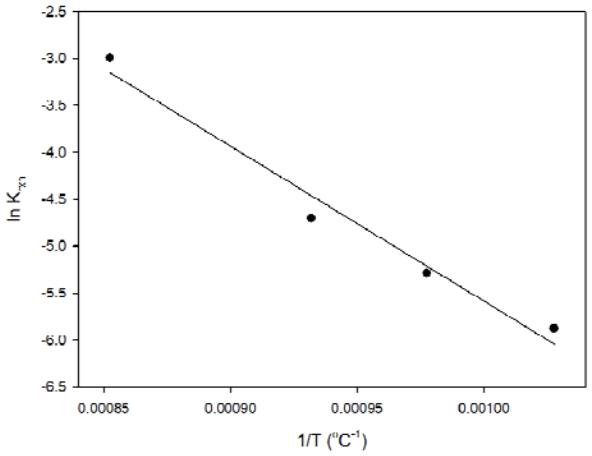

Figure 9. Arrhenius plots for the estimation of apparent activation energy

of the carbon source (ethanol), in order to obtain the required yield and quality of MLG using a CVD reactor.

Acknowledgment

The authors wish to acknowledge the funding from Malaysia's Ministry of Higher Education (MOHE), provided through the Fundamental Research Grant Scheme (FRGS) Vot. No. 5524471.

References

[1] Novoselov, K.S., Geim, A.K., Morozov, S.V., Jiang, D., Zhang, Y., Dubonos, S.V., Novoselov, K. S, Geim, A.K., Morozov, S.V., Jiang, D., Zhang, Y., Dubonos, S.V., Grigorieva, I.V., Firsov, A.A. (2011). Electric Field Effect in Atomically Thin Carbon Films. *Science*, 306(5696): 666-669. doi:10.1126/science. 1102896.

[2] Wang, G., Yang, J., Park, J., Gou, X., Wang, B., Liu, H., Wang, G., Yang, J., Park, J., Gou, X., Wang, B., Liu, H., Yao, J. (2008). Facile Synthesis and Characterization of Graphene Nanosheets. *J. Phys. Chem. B.* 112: 8192-8195. doi:10.1021/jp710931h.

[3] Singh, V., Joung, D., Zhai, L., Das, S., Khondaker, S.I., Seal, S. (2011). Graphene Based Materials: Past, Present and Future. *Prog. Mater. Sci.* 56: 1178-1271. doi:10.1016/ j.pmatsci.2011.03.003.

[4] Lightcap, I.V., Kosel, T.H., Kamat, P.V. (2010). Anchoring Semiconductor and Metal Nanoparticles on a Two-dimensional Catalyst Mat. Storing and Shuttling Electrons with Reduced Graphene Oxide. *Nano Lett.* 10: 577-583. doi:10.1021/nl9035109.

[5] Williams, G., Kamat, P.V. (2009). Graphene-semiconductor Nanocomposites: Excited-state Interactions Between ZnO Nanoparticles and Graphene Oxide. *Langmuir*. 25: 13869-13873. doi:10.1021/la900905h.

[6] Moon, J.S., Antcliffe, M., Seo, H.C., Lin, S.C., Schmitz, A., Milosavljevic, I., Moon, J.S., Antcliffe, M., Seo, H.C., Lin, S.C., Schmitz, A., Milosavljevic, I., McCalla, K., Wong, D., Gaskill, D.K,, Campbell, P.M., Lee, K.M. (2012). Graphene Review: An Emerging RF Technology. *2012 IEEE 12th Top Meet Silicon Monolith Integr. Circuits RF Syst. SiRF 2012 - Dig Pap*. 199-202. doi:10.1109/ SiRF.2012.6160170.

[7] Lian, P., Zhu, X., Liang, S., Li, Z., Yang, W., Wang, H. (2010). Large Reversible Capacity of High Quality Graphene Sheets as an Anode Material for Lithium-ion Batteries. *Electrochim. Acta.* 55: 3909-3914. doi:10.1016/ j.electacta.2010.02.025.

[8] Yu, J., Liu, G., Sumant, A.V., Goyal, V., Balandin, A.A. (2012). Graphene-on-diamond Devices with Increased Current-Carrying Capacity: Carbon sp 2-on-sp 3 Technology. *Nano Lett.* 12: 1603-1608. doi:10.1021/nl204545q.

[9] Bao, Q., Loh, K.P. (2012). Graphene Photonics, Plasmonics, and Broadband Optoelectronic Devices. *ACS Nano.* 6: 3677-–3694. doi:10.1021/nn300989g.

[10] Sun, Z., Hasan, T., Torrisi, F., Popa, D., Privitera, G., Wang, F., Sun, Z., Hasan, T., Torrisi, F., Popa, D., Privitera, G., Wang, F., Bonaccorso, F., Basko, D.M., Ferrari, A.C. (2010). Graphene Mode-locked Ultrafast Laser. *ACS Nano*. 4: 803-810. doi:10.1021/ nn901703e.

[11] Liu, M., Yin, X., Zhang, X. (2012). Double-layer Graphene Optical Modulator. *Nano Lett.* 12: 1482-1485. doi:10.1021/nl204202k.

[12] Soldano, C., Mahmood, A., Dujardin, E. (2010). Production, Properties and Potential of Graphene. *Carbon N. Y.* 48: 2127-2150. doi:10.1016/j.carbon.2010.01.058.

[13] Lemme, M.C., Echtermeyer, T.J., Baus, M., Kurz, H. (2007). A Graphene Field-effect Device. *IEEE Electron Device Lett.* 28: 282–284. doi:10.1109/LED.2007.891668.

[14] Chen, X., Akinwande, D., Lee, K.J., Close, G.F., Yasuda, S., Paul, B.C., Chen, X., Akinwande, D., Lee, K.J., Close, G.F., Yasuda, S., Paul, B.C., Fujita, S., Kong, J., Wong, H.S.P. (2010). Fully Integrated Graphene and Carbon Nanotube Interconnects for Gigahertz High-speed CMOS Electronics. *IEEE Trans Electron Devices.* 57: 3137-3143. doi:10.1109/ TED.2010.2069562.

[15] Terrones, M., Botello-Méndez, A.R., Campos-Delgado, J., López-Urías, F., Vega-Cantú, Y.I., Rodríguez-Macías, F.J., Terrones, M., Botello-Méndez, A.R., Campos-Delgado, J., López-Urías, F., Vega-Cantú, Y.I., Rodríguez-Macías, F.J., Elías, A.L., Munoz-Sandoval, E., Cano-Márquez, A.G., Charlier, J.C., Terrones, H. (2010). Graphene and Graphite Nanoribbons: Morphology, Properties, Synthesis, Defects and Applications. *Nano Today.* 5: 351-372. doi:10.1016/j.nantod.2010.06.010.

[16] Kaminska, I., Das, M.R., Coffinier, Y., Niedziolka-Jonsson, J., Sobczak, J., Woisel, P., Kaminska, I., Das, M.R., Coffinier, Y., Niedziolka-Jonsson, J., Sobczak, J., Woisel, P., Lyskawa, J., Opallo, M., Boukherroub, R., Szunerits, S. (2012). Reduction and Functionalization of Graphene Oxide Sheets Using Biomimetic Dopamine Derivatives in One Step. *ACS Appl. Mater. Interfaces.* 4: 1016-1020. doi:10.1021/am201664n.

[17] Khalid, N.R., Hong, Z., Ahmed, E., Zhang, Y., Chan, H., Ahmad, M. (2012). Synergistic Effects of Fe and Graphene on Photocatalytic Activity Enhancement of TiO_2 under Visible Light. *Appl. Surf. Sci.* 258: 5827-5834. doi:10.1016/j.apsusc.2012.02.110.

[18] Zhao, Y., Zhan, L., Tian, J., Nie, S., Ning, Z. (2011). Enhanced Electrocatalytic Oxidation of Methanol on Pd/Polypyrrole-graphene in Alkaline Medium. *Electrochim Acta.* 56: 1967-1972. doi:10.1016/ j.electacta.2010.12.005.

[19] Wang, G., Wang, B., Park, J., Wang, Y., Sun, B., Yao, J. (2009). Highly Efficient and Large-scale Synthesis of Graphene by Electrolytic Exfoliation. *Carbon N. Y.* 47: 3242-3246. doi:10.1016/j.carbon.2009.07.040.

[20] Stankovich, S., Dikin, D.A., Piner, R.D., Kohlhaas, K.A., Kleinhammes, A., Jia, Y., Stankovich, S., Dikin, D.A., Piner, R.D., Kohlhaas, K.A., Kleinhammes, A., Jia, Y., Wu, Y., Nguyen, S.T., Ruoff, R.S. (2007). Synthesis of Graphene-based Nanosheets via Chemical Reduction of Exfoliated Graphite Oxide. *Carbon N. Y.* 45: 1558-1565. doi:10.1016/j.carbon. 2007.02.034.

[21] Mattevi. C., Kim, H., Chhowalla, M. (2011). A Review of Chemical Vapour Deposition of Graphene on Copper. *J. Mater. Chem.* 21: 3324–3334. doi:10.1039/C0JM02126A.

[22] Yi, M., Shen, Z. (2015). A Review on Mechanical Exfoliation for the Scalable Production of Graphene. *J. Mater. Chem. A.* 3: 11700–11715. doi:10.1039/C5TA00252D.

[23] Chen, J., Duan, M., Chen, G. (2012). Continuous Mechanical Exfoliation of Graphene Sheets via Three-roll Mill. *J. Mater. Chem.* 22: 19625. doi:10.1039/c2jm33740a.

[24] Qian, W., Hao, R., Hou, Y., Tian, Y., Shen, C., Gao, H., Qian, W., Hao, R., Hou, Y., Tian, Y., Shen, C., Gao, H., Liang, X. (2009). Solvothermal-assisted Exfoliation Process to Produce Graphene with High Yield and High Quality. *Nano Res.* 2: 706-712. doi:10.1007/s12274-009-9074-z.

[25] Gilje, S., Han, S., Wang, M., Wang, K.L., Kaner, R.B. (2007). A Chemical Route to Graphene for Device Applications. *Nano Lett.* 7: 3394-3398. doi:10.1021/nl0717715.

[26] Robinson, J.T., Perkins, F.K., Snow, E.S., Wei, Z., Sheehan, P.E. (2008). Reduced Graphene Oxide Molecular Sensors. *Nano Lett.* 8: 3137–3140. doi:10.1021/nl8013007.

[27] Marcano, D.C., Kosynkin, D.V., Berlin, J.M., Sinitskii, A., Sun, Z., Slesarev, A., Marcano, D.C., Kosynkin, D.V., Berlin, J.M., Sinitskii, A., Sun, Z., Slesarev, A., Alemany, L.B., Lu, W., Tour, J.M. (2010). Improved Synthesis of Graphene Oxide. *ACS Nano.* 4: 4806-4814. doi:10.1021/nn1006368.

[28] Loh, K.P., Bao, Q., Ang, P.K. and Yang, J. (2010). The Chemistry of Graphene. *Journal of Materials Chemistry*, 20(12): 2277-2289. doi:10.1039/B920539J.

[29] Wei, D., Liu, Y., Wang, Y., Zhang, H., Huang, L., Yu, G. (2009). Synthesis of N-doped Graphene by Chemical Vapor Deposition and Its Electrical Properties. *Nano Lett.* 9: 1752–1758. doi:10.1021/nl803279t.

[30] Shahil, K.M.F., Balandin, A.A. (2012). Thermal Properties of Graphene and Multilayer Graphene: Applications in Thermal Interface Materials. *Solid State Commun.* 152: 1331–1340. doi:10.1016/j.ssc.2012.04.034.

[31] Batzill, M. (2012). The Surface Science of Graphene: Metal Interfaces, CVD Synthesis, Nanoribbons, Chemical Modifications, and Defects. *Surf. Sci. Rep.* 67: 83-115. doi:10.1016/j.surfrep.2011.12.001.

[32] Wang, Y., Xu, X., Lu, J., Lin, M., Bao, Q., Özyilmaz, B., Wang, Y., Xu, X., Lu, J., Lin, M., Bao, Q., Ozyilmaz, B., Loh, K.P. (2010). Toward High Throughput Interconvertible Graphane-to-graphene Growth and Patterning. *ACS Nano.* 4: 6146-6152. doi:10.1021/ nn1017389.

[33] Ogawa, S., Yamada, T., Ishidzuka, S., Yoshigoe, A., Hasegawa, M., Teraoka, Y., Ogawa, S., Yamada, T., Ishidzuka, S., Yoshigoe, A., Hasegawa, M., Teraoka, Y., Takakuwa, Y. (2013). Graphene Growth and Carbon Diffusion Process during Vacuum Heating on Cu (111)/Al_2O_3 Substrates. *Jpn. J. Appl. Phys.* 52: 110122.

[34] Liu, J., Tao, L., Yang, W., Li, D., Boyer, C., Wuhrer, R., Liu, J., Tao, L., Yang, W., Li, D., Boyer, C., Wuhrer, R., Braet, F., Davis, T.P. (2010). Synthesis, Characterization, and Multilayer Assembly of pH Sensitive Graphene-polymer Nanocomposites. *Langmuir.* 26: 10068-10075. doi:10.1021/la1001978.

[35] Liu, W-W., Chai, S-P., Mohamed, A.R., Hashim, U. (2014). Synthesis and Characterization of Graphene and Carbon Nanotubes: A Review on the Past and Recent Developments. *J. Ind. Eng. Chem.* 20: 1171–1185. doi:10.1016/j.jiec.2013.08.028.

[36] Zhao, H., Hui, K.S., Hui, K.N. (2014). Synthesis of Nitrogen-doped Multilayer Graphene from Milk Powder with Melamine and their Application to Fuel Cells. *Carbon N. Y.* 76: 1–9. doi:10.1016/j.carbon.2014.04.007.

[37] Calizo, I., Balandin, A.A., Bao, W., Miao, F., Lau, C.N. (2007). Temperature Dependence of the Raman Spectra of Graphene and Graphene Multilayers. *Nano Lett.* 7: 2645–2649. doi:10.1021/nl071033g.

[38] Burton, A.W., Ong, K., Rea, T., Chan, I.Y. (2009). On the Estimation of Average Crystallite Size of Zeolites from the Scherrer Equation: A Critical Evaluation of Its Application to Zeolites with One-dimensional Pore Systems. *Microporous Mesoporous Mater.* 117: 75-90. doi:10.1016/j.micromeso.2008.06.010.

[39] Calizo, I., Miao, F., Bao, W., Lau, C.N., Balandin, A.A. (2007). Variable Temperature Raman Microscopy as a Nanometrology Tool for Graphene Layers and Graphene-based Devices. *Appl. Phys. Lett.* 91: 3-5. doi:10.1063/1.2771379.

[40] Zhang, Y-H., Chen, Y-B., Zhou, K-G., Liu, C-H., Zeng, J., Zhang, H-L., Zhang, Y.H., Chen, Y.B., Zhou, K.G., Liu, C.H., Zeng, J., Zhang, H.L., Peng, Y. (2009). Improving Gas Sensing Properties of Graphene by Introducing Dopants and Defects: A First-principles Study. *Nanotechnology*. 20: 185504. doi:10.1088/0957-4484/20/18/185504.

[41] Zhu, Y., Murali, S., Cai, W., Li, X., Suk, J.W., Potts, J.R., Zhu, Y., Murali, S., Cai, W., Li, X., Suk, J.W., Potts, J.R., Ruoff, R.S. (2010). Graphene and Graphene Oxide: Synthesis, Properties, and Applications. *Adv. Mater.* 22: 3906-3924. doi:10.1002/adma.201001068.

[42] Zhong, C., Wang, J.Z., Wexler, D., Liu, H.K. (2014). Microwave Autoclave Synthesized Multi-layer Graphene/Single-walled Carbon Nanotube Composites For Free-standing Lithium-ion Battery Anodes. *Carbon N. Y.* 66: 637–645. doi:10.1016/j.carbon.2013.09.060.

[43] Choudhury, D., Das, B., Sarma, D.D., Rao, C.N.R. (2010). XPS Evidence for Molecular Charge-transfer Doping of Graphene. *Chem. Phys. Lett.* 497: 66–69. doi:10.1016/j.cplett.2010.07.089.

[44] Eda, B.G., Lin, Y., Mattevi, C., Yamaguchi, H., Chen, H., Chen, I., Eda, G., Lin, Y.Y., Mattevi, C., Yamaguchi, H., Chen, H.A., Chen, I.S.C.W., Chen, C.W., Chhowalla, M. (2010). Blue Photoluminescence from Chemically Derived Graphene Oxide. *Adv. Mater.* 22: 505-509. doi:10.1002/adma.200901996.

[45] Zhou, F., Sun, W., Ricardo, K.B., Wang, D., Shen, J., Yin, P., Zhou, F., Sun, W., Ricardo, K.B., Wang, D., Shen, J., Yin, P., Liu, H. (2016). Programmably Shaped Carbon Nanostructure from Shape-Conserving Carbonization of DNA. *ACS Nano.* 10: 3069-3077. doi:10.1021/acsnano.5b05159.

[46] Geng, Y., Wang, S.J., Kim, J.K. (2009). Preparation of Graphite Nanoplatelets and Graphene Sheets. *J. Colloid Interface Sci.* 336: 592–598. doi:10.1016/j.jcis.2009.04.005.

[47] Malard, L.M., Pimenta, M.A., Dresselhaus, G., Dresselhaus, M.S. (2009). Raman Spectroscopy in Graphene. *Phys. Rep.* 473: 51-87. doi:10.1016/j.physrep.2009.02.003.

[48] Das, A., Chakraborty, B., Sood, A.K. (2008). Raman Spectroscopy of Graphene on Different Substrates and Influence of Defects. *Bull. Mater. Sci.* 31: 579–584. doi:10.1007/s12034-008-0090-5.

[49] Yuan, W., Li, C., Li, D., Yang, J., Zeng, X. (2011). Preparation of Single-and Few-layer Graphene Sheets Using Co Deposition on Sic Substrate. *J. Nanometer.* 2011. doi:10.1155/2011/319624.

[50] Niilisk, A., Kozlova, J., Alles, H., Aarik, J., Sammelselg, V. (2016). Raman Characterization of Stacking in Multi-layer Graphene Grown on Ni. *Carbon N. Y.* 98: 658–665. doi:10.1016/j.carbon.2015.11.050.

[51] Nguyen, V.T., Le, H.D., Nguyen, V.C., Tam Ngo, T.T., Le, D.Q., Nguyen, X.N., Le, H.D., Ngo, T.T.T., Le, D.Q., Nguyen, X.N., Phan, N.M. (2013). Synthesis of Multi-layer Graphene Films on Copper Tape by Atmospheric Pressure Chemical Vapor Deposition Method. *Adv. Nat. Sci. Nanosci. Nanotechnol.* 4: 35012. doi:10.1088/2043-6262/4/3/035012.

[52] Shokrian, M., Sadrzadeh, M., Mohammadi, T. (2010). C_3H_8 Separation from CH_4 and H_2 using a Synthesized PDMS Membrane: Experimental and Neural Network Modeling. *J. Memb. Sci.* 346: 59-70. doi:10.1016/j.memsci.2009.09.015.

[53] Senum, G.I., Yang, R.T. (1977). Rational Approximations of the Integral of the Arrhenius Function. *J. Therm. Anal.* 11: 445-447. doi:10.1007/BF01903696.

[54] Ayodele, B.V., Khan, M.R., Lam, S.S., Cheng, C.K. (2016). Production of CO-rich Hydrogen from Methane Dry Reforming over Lanthania-supported Cobalt Catalyst: Kinetic and Mechanistic Studies. *Int. J. Hydrogen Energy.* doi:10.1016/j.ijhydene.2016.01.091.

[55] Losurdo, M., Giangregorio, M.M., Capezzuto, P., Bruno, G. (2011). Graphene CVD Growth on Copper and Nickel: Role of Hydrogen in Kinetics and Structure. *Phys. Chem. Chem. Phys.* 13: 20836. doi:10.1039/c1cp22347j.

[56] Kim, H., Mattevi, C., Calvo, M.R., Oberg, J.C., Artiglia, L., Agnoli, S., Kim, H., Mattevi, C., Calvo, M.R., Oberg, J.C., Artiglia, L., Agnoli, S., Hirjibehedin, C.F., Chhowalla, M., Saiz, E. (2012). Activation Energy Paths for Graphene Nucleation and Growth on Cu. *ACS Nano.* 6: 3614-3623. doi:10.1021/nn3008965.